



NRC Publications Archive Archives des publications du CNRC

Raman-induced slow-light delay of THz-bandwidth pulses

Bustard, Philip J.; Heshami, Khabat; England, Duncan G.; Spanner, Michael; Sussman, Benjamin J.

This publication could be one of several versions: author's original, accepted manuscript or the publisher's version. / La version de cette publication peut être l'une des suivantes : la version prépublication de l'auteur, la version acceptée du manuscrit ou la version de l'éditeur.

For the publisher's version, please access the DOI link below. / Pour consulter la version de l'éditeur, utilisez le lien DOI ci-dessous.

Publisher's version / Version de l'éditeur:

<https://doi.org/10.1103/PhysRevA.93.043810>

Physical Review A, 93, 4, 2016-04-06

NRC Publications Record / Notice d'Archives des publications de CNRC:

<https://nrc-publications.canada.ca/eng/view/object/?id=5ccb84b2-0cdc-4835-a7bd-e167ece89a9d>

<https://publications-cnrc.canada.ca/fra/voir/objet/?id=5ccb84b2-0cdc-4835-a7bd-e167ece89a9d>

Access and use of this website and the material on it are subject to the Terms and Conditions set forth at

<https://nrc-publications.canada.ca/eng/copyright>

READ THESE TERMS AND CONDITIONS CAREFULLY BEFORE USING THIS WEBSITE.

L'accès à ce site Web et l'utilisation de son contenu sont assujettis aux conditions présentées dans le site

<https://publications-cnrc.canada.ca/fra/droits>

LISEZ CES CONDITIONS ATTENTIVEMENT AVANT D'UTILISER CE SITE WEB.

Questions? Contact the NRC Publications Archive team at

PublicationsArchive-ArchivesPublications@nrc-cnrc.gc.ca. If you wish to email the authors directly, please see the first page of the publication for their contact information.

Vous avez des questions? Nous pouvons vous aider. Pour communiquer directement avec un auteur, consultez la première page de la revue dans laquelle son article a été publié afin de trouver ses coordonnées. Si vous n'arrivez pas à les repérer, communiquez avec nous à PublicationsArchive-ArchivesPublications@nrc-cnrc.gc.ca.



Raman-induced slow-light delay of THz-bandwidth pulses

Philip J. Bustard,¹ Khabat Heshami,¹ Duncan G. England,¹ Michael Spanner,¹ and Benjamin J. Sussman^{1,2,*}

¹National Research Council of Canada, 100 Sussex Drive, Ottawa, Ontario, K1A 0R6 Canada

²Department of Physics, University of Ottawa, Ottawa, Ontario, K1N 6N5 Canada

(Received 24 July 2015; revised manuscript received 19 January 2016; published 6 April 2016)

We propose and experimentally demonstrate a scheme to generate optically controlled delays based on off-resonant Raman absorption. Dispersion in a transparency window between two neighboring, optically activated Raman absorption lines is used to reduce the group velocity of broadband 765 nm pulses. We implement this approach in a potassium titanyl phosphate (KTP) waveguide at room temperature, and demonstrate Raman-induced delays of up to 140 fs for a 650-fs duration, 1.8-THz bandwidth, pulse. Our approach should be applicable to single-photon signals, offers wavelength tunability, and is a step toward processing ultrafast photons.

DOI: [10.1103/PhysRevA.93.043810](https://doi.org/10.1103/PhysRevA.93.043810)

I. INTRODUCTION

The effective operation of communication networks requires the ability to buffer and control the movement of information, whether in a postal service [1] or a quantum network [2]. All-optical controls are particularly desirable for classical and quantum photonic communication systems because manipulations can be effected rapidly, enabling high-bandwidth operations. The need for photonic propagation controls has motivated much research toward the development of slow-light devices. These technologies modify the dispersion relationship between photon energy and momentum to reduce the group velocity of optical pulses, for example, using dispersion close to a reflection resonance in periodically structured photonic media, or material dispersion associated with optical resonance features causing gain or loss [3]. Potential network applications of slow light include optical switching, signal synchronization, and buffering for all-optical routers [4]. In addition, slow light offers the prospect of improved optical sensing [5] and enhanced nonlinear interactions [6–8].

Periodically structured media slow light near reflection resonances, where energy is transferred between strongly coupled forward- and backward-propagating waves, thereby reducing the group velocity [6]. Bragg gratings offer a simple implementation; however, more sophisticated coupled resonator structures are necessary to reduce the group velocity while minimizing higher-order dispersion which distorts the shape of pulses. For example, cascaded Bragg gratings [9], Moiré gratings [10,11], ring resonators [12], and photonic crystal structures [13–17] have all been used to demonstrate slow light. However, such structures offer limited tunability and lack continuous optical control when compared with optical absorption and gain resonance techniques.

Slow light has been achieved for pulses tuned between absorbing resonances in an atomic vapor [18–22]. In one demonstration, pulses as short as 275 ps were delayed by up to 6.8 ns [19]. Motivated by the desire for optical control of slow light, a variety of nonlinear phenomena have been exploited, including stimulated Brillouin scattering (SBS) [23,24], stimulated Raman scattering (SRS) [25], and electromagnetically induced transparency (EIT) [26,27]. In

EIT, a control field opens a narrow transparency window within an absorption line. The steep dispersion in the transparency window strongly reduces the group velocity of probe radiation, and the resulting slow light can be used to produce efficient nonlinear interactions [7,8]; however, linewidth limitations typically restrict the use of EIT to narrow-band pulses with MHz bandwidth [28]. Alternative methods which use gain features arising from SBS [23] and SRS [25] in optical fiber have been demonstrated with higher-bandwidth pulses, with input durations of 15 ns and 430 fs, respectively. Techniques which use gain can produce noise photons; such methods are therefore unsuitable for quantum information and communication protocols which rely on photon counting. Furthermore, use of a fiber-based technique over km propagation distances [25] will chirp femtosecond pulses to many picoseconds in duration, and will add a large fixed delay, thereby limiting the potential speed in optical processing applications. As an alternative to slow light, Raman quantum memories can control the group delay of ultrafast pulses [29,30], but only for delays longer than the pulse duration because of constraints on the necessary control pulses.

II. THE SCHEME

In this paper, we propose and experimentally demonstrate an all-optical scheme for slow light, suitable for ultrabroadband single photons. Our technique is broadly tunable and can be implemented in molecular ensembles, atomic vapors, and solids. The scheme reduces the group velocity of ultrabroadband *signal* photons using off-resonant Raman absorption. As shown in Fig. 1(a), the signal pulse of frequency ω_{sig} copropagates with a strong, near-constant intensity, *control* pulse of frequency ω_c through a medium with a double- Λ -level structure. Dipole transitions between the three lower states and the upper manifold of states $|m\rangle$ are permitted, resulting in Raman coupling of levels $|1\rangle \rightarrow |2\rangle$ and $|1\rangle \rightarrow |3\rangle$ when the control and signal pulses are applied. The gradient in linear dispersion between two absorption lines can be used to reduce or increase the group velocity of light [18,20]. Here, this is achieved for the signal field by setting $(\omega_{\text{sig}} - \omega_c) = \omega_2 - \omega_1 + \Delta/2 = \omega_3 - \omega_1 - \Delta/2$, where $\hbar\Delta$ is the energy splitting of levels $|2\rangle$ and $|3\rangle$, and $\hbar\omega_k$ is the energy of level $|k\rangle$. The control and signal pulses have bandwidths $\delta\omega_c$ and $\delta\omega_{\text{sig}}$, respectively, satisfying

*ben.sussman@nrc.ca

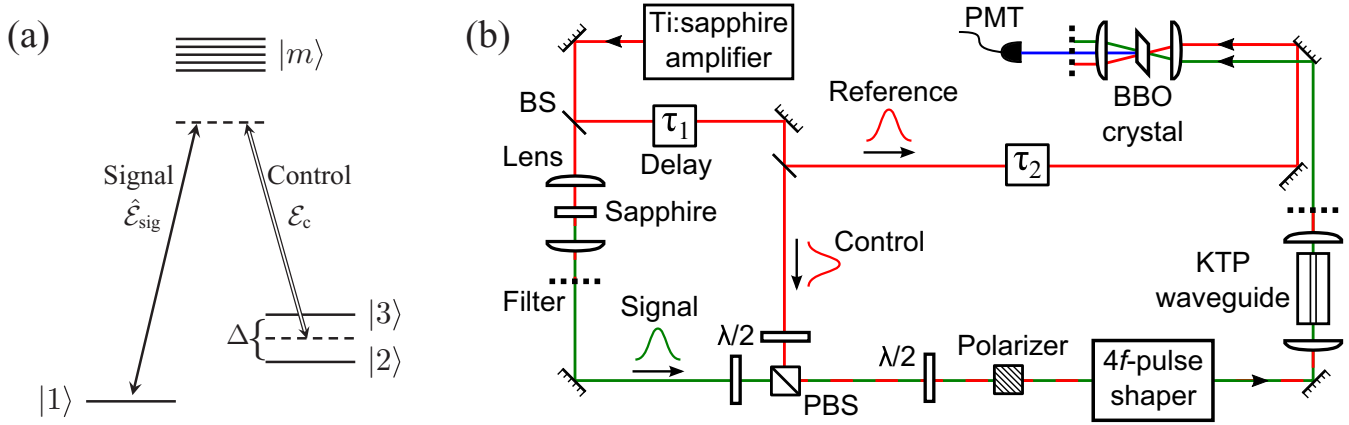


FIG. 1. (a) The generic level configuration and (b) the experimental layout of our scheme. The signal field is coupled near two-photon resonance with two Raman-accessible states ($|2\rangle$ and $|3\rangle$).

$\delta\omega_c \ll \delta\omega_{\text{sig}} < \Delta$ such that the control pulse intensity is near constant for the duration of the signal pulse. The signal pulse experiences dispersion from each of the two Raman absorption lines, but absorption losses are minimized by the detuning from two-photon resonance. The use of two Raman lines, rather than one, ensures that the absorption is approximately constant, and the dispersion increases approximately linearly, across the signal pulse spectrum. As a result, the signal group velocity is reduced evenly: higher-order dispersion and uneven absorption, which distort the pulse shape, are kept to a minimum. This Raman scheme enables fast control and broad tunability of the dispersion by switching the intensity and wavelength of the control pulse. In contrast to slow-light techniques which involve gain in an amplifier, we expect this scheme to be suitable for controlling single-photon pulses while maintaining their quantum character. The speed and quantum compatibility of this method make it an attractive tool for pulse sequencing in quantum key distribution, for example [31,32].

III. EXPERIMENT

The layout of our experiment is shown in Fig. 1(b). The signal and control pulses are generated using a Coherent RegA Ti:sapphire laser system which outputs 160 fs pulses, centered at 795 nm, at a repetition rate of 49 kHz. The beam is partitioned at a beam splitter (BS) and the transmitted beam is focused into a sapphire plate to generate a white-light continuum spectrum by self-phase modulation [33]; the white-light spectrum is spatially and spectrally filtered to create the signal pulse for the slow-light interaction. The beam reflected by the beam splitter is sent to an optical delay line (τ_1). This beam is subsequently partitioned to create a control pulse for the slow-light interaction and a *reference* pulse; the reference pulse, duration $\tau_{\text{ref}} \approx 160$ fs, is sent to a cross-correlator with variable delay (τ_2) for measurement of the slow light. The signal and control beams are combined at a polarizing beam splitter (PBS) and sent through an amplitude $4f$ pulse shaper which allows independent spectral control of each beam by translating knife edges in the focal plane of the shaper [34]. We spectrally filter the control

spectrum to < 1 nm bandwidth, centered at $\lambda_c = 795$ nm; the control pulse has a full width at half maximum (FWHM) duration of $\tau_c = 4$ ps. With no filtering in the $4f$ shaper, the signal spectrum spans the range $755 \lesssim \lambda_{\text{sig}} \lesssim 780$ nm. After filtering, the signal pulse has a FWHM bandwidth of 3.6 nm, corresponding to a Fourier-limited pulse duration of $\tau_{\text{sig}}^{\text{FL}} \approx 490$ fs. The control pulse, energy $\mathcal{E}_c = 14.3(8)$ nJ, and signal pulse, energy $\mathcal{E}_{\text{sig}} = 40(1)$ pJ, are then focused into a 3-cm-long potassium titanyl phosphate (KTP) single-mode waveguide [35,36]. At the output of the waveguide, the beam is collimated and sent to a spectrometer (Ocean Optics HR4000) or to a background-free, noncollinear, cross-correlation setup [34]. The cross-correlation setup allows measurement of the signal pulse arrival time and temporal intensity profile by type-I sum-frequency generation (SFG) with the reference pulse in a 200- μm -thick beta barium borate (BBO) crystal. The SFG cross-correlation signal is detected using a photomultiplier tube (PMT) and boxcar integrated for data acquisition.

The KTP crystal is Z cut, with a waveguide written in the X direction; the mode field diameter is $\sim 4 \mu\text{m}$. The control and signal pulses propagate in the X direction, each with Z polarization. In this configuration [X(ZZ)X], KTP exhibits multiple vibrational Raman peaks in the Stokes spectrum on the interval from ~ 50 to $\sim 850 \text{ cm}^{-1}$ shift [37,38]. In Fig. 2, we plot the signal Raman absorption spectrum between 758 and 778 nm, measured by temporally overlapping the unfiltered signal pulse with the control pulse in the waveguide. The Raman absorption $\mathcal{A}(\lambda)$ is given by $\mathcal{A}(\lambda) = 1 - I_{\text{sig}}^{\text{on}}(\lambda)/I_{\text{sig}}^{\text{off}}(\lambda)$, where $I_{\text{sig}}^{\text{off}}(\lambda)$ ($I_{\text{sig}}^{\text{on}}(\lambda)$) is the signal spectral intensity at wavelength λ output from the waveguide with the control pulse off (on). The spectrum shows absorption peaks at 759.4 and 772.4 nm, separated by a “window” of lower absorption in the range $763 \lesssim \lambda_{\text{sig}} \lesssim 768$ nm. This absorption structure replicates the doublet required for Raman slow light. The $4f$ pulse shaper is used to filter the signal spectrum to fit in the absorption window as shown in Fig. 2 (control pulse off, dashed blue curve); when the control pulse is turned on (solid green curve), the signal intensity is reduced by $\approx 35\%$ due to Raman absorption.

In Fig. 3, we plot the normalized intensity cross correlation of the signal pulse with the control pulse on and off. The cross correlation has a FWHM duration of $\tau_{\text{xc}} = 675$ fs, giving a

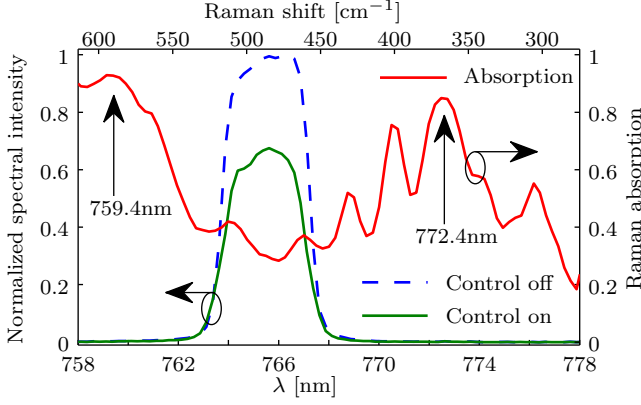


FIG. 2. Right-hand ordinate: plot of the measured Raman absorption spectrum of the KTP waveguide (red curve) showing absorption peaks at 759.4 and 772.4 nm. Left-hand ordinate: the signal spectrum, prefiltered in the $4f$ shaper and measured at the output of the waveguide, is plotted with the 795 nm control pulse off (blue dashed curve) and on (green solid curve), showing that the control pulse causes Raman absorption of the signal pulse.

signal pulse duration of $\tau_{\text{sig}} \approx (\tau_{\text{xc}}^2 - \tau_{\text{ref}}^2)^{1/2} = 650$ fs, such that $\tau_{\text{sig}} > \tau_{\text{sig}}^{\text{FL}}$ because the signal is chirped by dispersion in the waveguide. Figure 3 shows that the normalized cross correlation with the control pulse on (green solid curve) is delayed in time relative to the case with the control pulse off (blue dashed curve). The mean pulse delay can be measured by the first moment, or mean, of the cross-correlation intensity,

$$\langle \tau \rangle = \frac{\int \tau I(\tau) d\tau}{\int I(\tau) d\tau} \Big|_{\text{control on}} - \frac{\int \tau I(\tau) d\tau}{\int I(\tau) d\tau} \Big|_{\text{control off}},$$

where $I(\tau)$ is the cross-correlation intensity as a function of the delay τ between the signal and reference pulses. In the inset of Fig. 3, we plot the mean pulse delay $\langle \tau \rangle$ as a function

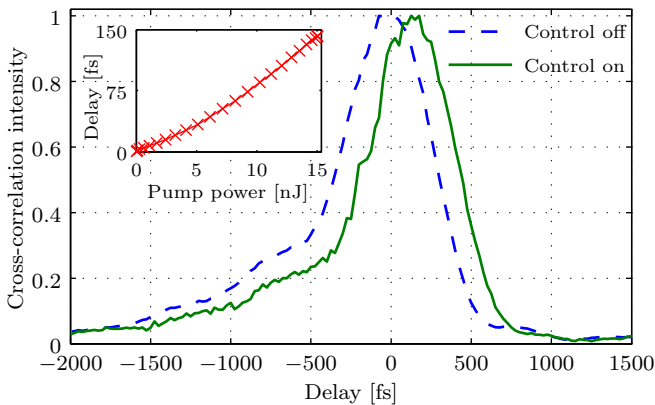


FIG. 3. Plot of the normalized cross-correlation intensity between the reference pulse and the signal pulse output from the waveguide with the control pulse off (dashed blue curve) and on (solid green curve). The signal pulse is delayed relative to the reference pulse due to Raman interaction with the control pulse. Inset: a plot of the signal delay as a function of control power, measured using the first moment of the cross-correlation intensity $\langle \tau \rangle$; we measure delays of up to 140 fs.

of the input control pulse energy, showing a smooth increase in the delay from zero up to 140 fs at the maximum control pulse energy of 14.3(8) nJ.

IV. THEORY AND DISCUSSION

We model our scheme assuming an ensemble system with the level configuration shown in Fig. 1(a) with two Raman-accessible states ($|2\rangle$ and $|3\rangle$). The signal is optically coupled to these states, and the two-photon transition is tuned to a point between the two Raman absorption lines. By adiabatic elimination of the high-energy $|m\rangle$ states, and assuming that dipole transitions $|1\rangle \leftrightarrow |2\rangle$ and $|1\rangle \leftrightarrow |3\rangle$ are negligible, we derive the following Maxwell-Bloch equations for this system (see Appendix) [39,40]:

$$\dot{\hat{Q}}_{31}(z,t) = -\Gamma_3 \hat{Q}_{31}(z,t) - i\kappa_{13} E_c^*(z,t) \hat{E}_{\text{sig}}(z,t) e^{-i\frac{\Delta}{2}t}, \quad (1)$$

$$\dot{\hat{Q}}_{21}(z,t) = -\Gamma_2 \hat{Q}_{21}(z,t) - i\kappa_{12} E_c^*(z,t) \hat{E}_{\text{sig}}(z,t) e^{i\frac{\Delta}{2}t}, \quad (2)$$

$$\left(\partial_z + \frac{1}{c} \partial_t \right) \hat{E}_{\text{sig}}(z,t) = iE_c(z,t) [\beta_{31} \hat{Q}_{31}(z,t) e^{i\frac{\Delta}{2}t} + \beta_{21} \hat{Q}_{21}(z,t) e^{-i\frac{\Delta}{2}t}]. \quad (3)$$

Here, $\hat{E}_{\text{sig}}(z,t)$, $E_c(z,t)$, and $\hat{Q}_{ij}(z,t)$ are slowly varying components, respectively, of the signal field, control field, and coherences in the medium between states $|i\rangle$ and $|j\rangle$, as a function of propagation coordinate z and time t ; we ignore transverse field effects and consider propagation over a distance L . The frequency spacing between the two Raman lines is denoted by Δ , and $\Gamma_{2,3}$ are absorption linewidths; the coupling coefficients are $\kappa_{ij} = \sum_m d_{im} d_{mj} [(\omega_{mi} - \omega_{\text{sig}})^{-1} + (\omega_{mi} + \omega_c)^{-1}]$ and $\beta_{ij} = 2\pi N \hbar \kappa_{ij} / c$, where N is the number density and $d_{ij} = \langle i | \hat{d} | j \rangle / \hbar$ is the matrix element of the dipole operator \hat{d} . Note that we have assumed fixed population in the ground and Raman states because the population transfer is negligible with a weak signal field. We do not include additional Raman sidebands because the coupling strength is low, such that the control pulse is undepleted by stimulated Raman scattering.

Equations (1)–(3) can be solved numerically to demonstrate the Raman-induced group delay. However, the most important features of our scheme can be captured through an analytical solution by assuming a control field with constant intensity. As shown in the Appendix, we can analytically find the linear response function and consequently describe the loss and group delay as a function of the peak optical depth of the medium. Assuming that the absorption lines have the same Raman couplings and linewidths, such that $\kappa_{12} \beta_{21} = \kappa_{13} \beta_{31}$ and $\Gamma = \Gamma_2 = \Gamma_3$, respectively, we show that the group delay τ_g is given by

$$\tau_g = d_0 \frac{\Gamma(\Delta^2/4 - \Gamma^2)}{(\Delta^2/4 + \Gamma^2)^2},$$

with an associated loss in dB

$$\eta = d_0 \frac{10}{\ln(10)} \frac{2\Gamma^2}{\Delta^2/4 + \Gamma^2},$$

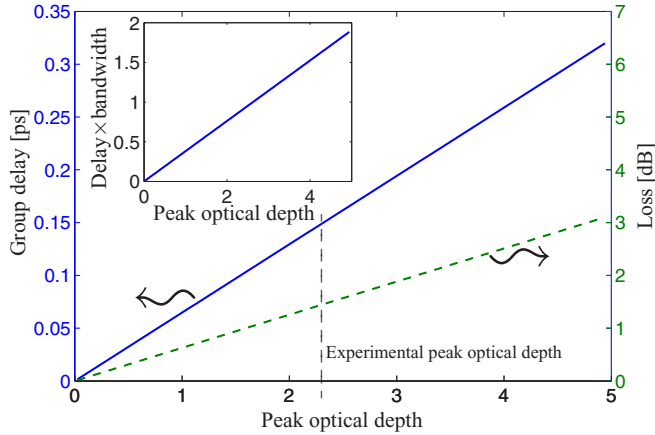


FIG. 4. Theoretical group delay and loss with respect to the Raman peak optical depth. We assume $\Gamma = 1$ THz and $\Delta = 6.8$ THz, such that the absorption and dispersion based on the model resemble that of the experiment; see Fig. 6 in the Appendix. The inset shows the theoretical delay-bandwidth product, where the bandwidth is $\Delta - \Gamma$.

where $d_0 = k_0 L \kappa_{12} \beta_{21} |E_c|^2 / \Gamma$ is the Raman peak optical depth in resonance with each Raman line, and k_0 is the wave vector of the signal frequency.

The expected group delay and loss are shown in Fig. 4 for $\Gamma = 1$ THz and $\Delta = 6.8$ THz as a function of the peak optical depth. The parameters Δ and Γ are chosen such that the response function (derived from our theoretical description) matches the measurement results; see Fig. 6 in the Appendix. The delay-bandwidth product can be defined as a more explicit measure of our scheme's performance. Assuming that the available bandwidth of the transparency window is given by $\Delta - \Gamma$, we plot the theoretical delay-bandwidth product in the inset of Fig. 4. A delay-bandwidth product of 1 means that the delay will be equal to the transform-limited signal duration if all of the available bandwidth is used. For our parameters, this can be achieved at $d_0 \approx 2.5$, which is demonstrated for one of the Raman absorption peaks in our experiment. The peak optical depth, and thus the maximum delay, in our experiment was limited by the available control pulse energy; however, the optical depth can be increased by use of a more powerful control pulse, or a longer KTP waveguide. Alternative Raman-active media may also enable larger peak optical depths. As the optical depth is increased, the control pulse will eventually be depleted by nonlinear generation of Stokes photons; this will ultimately limit the maximum possible group delay.

The measurement results in the inset of Fig. 3 for delay vs power slightly deviate from our predicted linear dependence shown in Fig. 4. This is because the Lorentzian line shapes used in the theoretical model result in negligible group delay dispersion (GDD) in the transparency window; however, in the experiment, the more complicated wavelength dependence of the absorption spectrum (see Fig. 2) causes GDD, which results in the nonlinear dependence of Fig. 3 (inset).

V. CONCLUSION

In summary, we have introduced a Raman-based scheme for generating optically induced slow light, and demonstrated it in

a KTP waveguide which provided a transparency window with approximately 5.8 THz of bandwidth. Using a signal pulse at 765 nm with 1.8 THz bandwidth, corresponding to a Fourier-limited pulse duration of 490 fs, we achieved power-dependent delays of up to 140 fsec.

The operational bandwidth of our scheme is determined by the medium; the delay depends on the control field intensity, frequency spacing between Raman levels, and Raman linewidths. Given that we use linear dispersion between two absorption lines, temporal delay is accompanied by loss. Delay per loss remains independent of the peak optical depth and only depends on the frequency spacing between the Raman absorption lines, and the Raman linewidths. For the theoretical parameters modeled, a delay-bandwidth product of 1 corresponds to ≈ 1.5 dB loss. The loss can be reduced by using a medium with narrower Raman linewidths.

In principle, due to the use of absorption features rather than gain features which add noise photons to the delayed signal pulse, our scheme can be implemented to process single photons. Furthermore, noise photons created by Raman scattering of control photons could be spectrally filtered to preserve the single-photon characteristics of the signal. Thanks to the off-resonant Raman coupling, the delay can be controlled optically, delivering frequency tunability, and the possibility of operating on multiple signals concurrently by frequency multiplexing. Alternative media with more Raman lines can also provide multimode functionality with one control field; for example, rovibrational manifolds of liquid or gas-phase molecular ensembles in hollow-core fibers are attractive candidate systems [41]. We expect that these multimode functionalities will find use in ultrafast quantum processing applications; for example, combining our scheme with a frequency shifter [42,43] provides the elements needed for an ultrafast optical pulse sequencer, similar to demonstrations using MHz-bandwidth pulses [44,45]. Alternatively, the scheme could be used to actively compensate, with high precision, for time drifts between photons interacting by two-photon interference in quantum information applications [46].

ACKNOWLEDGMENTS

The authors are grateful to Paul Hockett and Rune Lausten for comments on the manuscript. The authors wish to thank Philip Battle of AdvR Inc. This work was partly supported by NSERC (Canada).

P.J.B. and K.H. contributed equally to this work.

APPENDIX

1. Equations of motion

We describe here the equations of motion that are used for deriving the Maxwell-Bloch equations [39,40]. The total Hamiltonian (H_{tot}) driving the dynamics of the system includes the internal energy of states of the medium and interaction with electromagnetic fields based on the dipole approximation. Using the Heisenberg relation ($\frac{d\hat{O}}{dt} = \frac{i}{\hbar} [H_{\text{tot}}, \hat{O}] + \frac{\partial \hat{O}}{\partial t}$), one can derive the following set of equations:

$$\frac{d\hat{\rho}_{31}}{dt} = i\omega_{31}\hat{\rho}_{31} + i \sum_m (d_{1m}\hat{\rho}_{3m} - d_{m3}\hat{\rho}_{m1})\mathcal{E}_{\text{tot}}, \quad (\text{A1})$$

$$\frac{d\hat{\rho}_{21}}{dt} = i\omega_{21}\hat{\rho}_{21} + i \sum_m (d_{1m}\hat{\rho}_{2m} - d_{m2}\hat{\rho}_{m1})\mathcal{E}_{\text{tot}}, \quad (\text{A2})$$

$$\begin{aligned} \frac{d\hat{\rho}_{m1}}{dt} &= i\omega_{m1}\hat{\rho}_{m1} - id_{1m}\mathcal{E}_{\text{tot}}(\hat{\rho}_{11} - \hat{\rho}_{mm}) \\ &\quad - id_{3m}\mathcal{E}_{\text{tot}}\hat{\rho}_{31} - id_{2m}\mathcal{E}_{\text{tot}}\hat{\rho}_{21}, \end{aligned} \quad (\text{A3})$$

$$\frac{d\hat{\rho}_{3m}}{dt} = i\omega_{3m}\hat{\rho}_{3m} - id_{m3}\mathcal{E}_{\text{tot}}(\hat{\rho}_{mm} - \hat{\rho}_{33}) + id_{m1}\mathcal{E}_{\text{tot}}\hat{\rho}_{31}, \quad (\text{A4})$$

$$\frac{d\hat{\rho}_{2m}}{dt} = i\omega_{2m}\hat{\rho}_{2m} - id_{m2}\mathcal{E}_{\text{tot}}(\hat{\rho}_{mm} - \hat{\rho}_{22}) + id_{m1}\mathcal{E}_{\text{tot}}\hat{\rho}_{21}, \quad (\text{A5})$$

where $\hat{\rho}_{ij} = |i\rangle\langle j|$ and $\mathcal{E}_{\text{tot}} = \mathcal{E}_c(z,t) + \hat{\mathcal{E}}_{\text{sig}}(z,t)$. The function $\mathcal{E}_c(z,t) = E_c(z,t)e^{i(\omega_c t - k_c z)} + E_c^*(z,t)e^{-i(\omega_c t - k_c z)}$ denotes the control field and $\hat{\mathcal{E}}_{\text{sig}}(z,t) = \hat{E}_{\text{sig}}(z,t)e^{i(\omega_{\text{sig}} t - k_{\text{sig}} z)} + \hat{E}_{\text{sig}}^\dagger(z,t)e^{-i(\omega_{\text{sig}} t - k_{\text{sig}} z)}$ represents the signal field. The dipole matrix elements are $d_{ij} = \langle i|\hat{d}|j\rangle/\hbar$, and ω_{ij} is the angular frequency of the transition from $|j\rangle$ to $|i\rangle$. As shown in Fig. 1(a), the $|m\rangle$ states represent the excited-state manifold.

In order to eliminate the excited-state dynamics, we integrate equations (A3)–(A5) from the above set and use the result to rewrite the dynamics of $\hat{\rho}_{31}$ and $\hat{\rho}_{21}$. We neglect the Stark shift term and eliminate the fast-rotating terms compared to slowly varying components. For a scatterer at position z , this results in

$$\begin{aligned} \frac{d\hat{\rho}_{31}}{dt} &= i\omega_{31}\hat{\rho}_{31} - i\kappa_{13}E_c^*(z,t)\hat{E}_{\text{sig}}(z,t)e^{-i\frac{\Delta}{2}t} \\ &\quad \times (\hat{\rho}_{11} - \hat{\rho}_{33})e^{i\omega_{31}t}e^{i(k_c - k_{\text{sig}})z}, \end{aligned} \quad (\text{A6})$$

and

$$\begin{aligned} \frac{d\hat{\rho}_{21}}{dt} &= i\omega_{21}\hat{\rho}_{21} - i\kappa_{12}E_c^*(z,t)\hat{E}_{\text{sig}}(z,t)e^{i\frac{\Delta}{2}t} \\ &\quad \times (\hat{\rho}_{11} - \hat{\rho}_{22})e^{i\omega_{21}t}e^{i(k_c - k_{\text{sig}})z}, \end{aligned} \quad (\text{A7})$$

where

$$\kappa_{li} = \sum_m d_{1m}d_{mi} \left(\frac{1}{\omega_{m1} - \omega_{\text{sig}}} + \frac{1}{\omega_{m1} + \omega_c} \right).$$

We rewrite the above equations for slowly varying components (\hat{Q}_{ij}) of the matter coherences ($\hat{\rho}_{ij}$); this leads to

$$\frac{d\hat{Q}_{31}}{dt} = -\Gamma_3\hat{Q}_{31} - i\kappa_{13}(\hat{Q}_{11} - \hat{Q}_{33})E_c^*(z,t)\hat{E}_{\text{sig}}(z,t)e^{-i\frac{\Delta}{2}t}, \quad (\text{A8})$$

and

$$\frac{d\hat{Q}_{21}}{dt} = -\Gamma_2\hat{Q}_{21} - i\kappa_{12}(\hat{Q}_{11} - \hat{Q}_{22})E_c^*(z,t)\hat{E}_{\text{sig}}(z,t)e^{i\frac{\Delta}{2}t}, \quad (\text{A9})$$

where $\hat{Q}_{\nu 1}(t) = \hat{\rho}_{\nu 1}e^{-i\omega_{\nu 1}t}e^{-i(k_c - k_{\text{sig}})z}$ for $\nu = 2, 3$ and Γ_ν are linewidths associated to $|\nu\rangle$ Raman lines. We assume a cylindrically shaped ensemble of length L along the z (propagation) direction and we define collective operators by averaging over all scatterers with a slice of length Δz with N_z atoms (or molecules). Assuming that $N_z \gg 1$ and that all

of the scatterers are initially in state $|1\rangle$, we can simplify the above Bloch equations to

$$\dot{\hat{Q}}_{31}(z,t) = -\Gamma_3\hat{Q}_{31}(z,t) - i\kappa_{13}E_c^*(z,t)\hat{E}_{\text{sig}}(z,t)e^{-i\frac{\Delta}{2}t}, \quad (\text{A10})$$

$$\dot{\hat{Q}}_{21}(z,t) = -\Gamma_2\hat{Q}_{21}(z,t) - i\kappa_{12}E_c^*(z,t)\hat{E}_{\text{sig}}(z,t)e^{i\frac{\Delta}{2}t}. \quad (\text{A11})$$

Here, $\hat{Q}_{ij}(z,t) = \sum_{k=1}^{N_z} \hat{Q}_{ij}^{(k)}(t)$ and $\hat{Q}_{ij}^{(k)}(t)$ is the coherence operator for the k th atom in a slice of the ensemble at position z .

2. Propagation of EM fields

Propagation of the signal and control fields are determined by the total macroscopic polarization that these fields experience in the medium. We are interested in single-photon (weak) signal fields. The signal-field propagation is therefore given by the one-dimensional wave equation,

$$\left(\partial_z^2 - \frac{1}{c^2} \partial_t^2 \right) \hat{\mathcal{E}}_{\text{sig}}(z,t) = \frac{4\pi}{c^2} \partial_t^2 \hat{\mathcal{P}}_{\text{sig}}(z,t), \quad (\text{A12})$$

where

$$\hat{\mathcal{P}}_{\text{sig}}(z,t) = \frac{\hbar}{A\Delta z} \sum_{i=1}^{N_z} \sum_m [d_{1m}\hat{\rho}_{1m}^i + d_{m3}\hat{\rho}_{m3}^i + d_{m2}\hat{\rho}_{m2}^i]. \quad (\text{A13})$$

Similar to the derivation for Eqs. (A6) and (A7), and by keeping only terms that oscillate near the frequency of ω_{sig} , we find

$$\begin{aligned} \hat{\mathcal{P}}_{\text{sig}}(z,t) &= N\hbar E_c(z,t) [\kappa_{31}\hat{Q}_{31}(z,t)e^{i\frac{\Delta}{2}t} \\ &\quad + \kappa_{21}\hat{Q}_{21}(z,t)e^{-i\frac{\Delta}{2}t}] e^{i(\omega_{\text{sig}} t - k_{\text{sig}} z)}, \end{aligned} \quad (\text{A14})$$

where N is the number density per unit volume. One can simplify Eq. (A12) to the following first-order equation for the forward-propagating component of the signal field,

$$\begin{aligned} \left(\partial_z + \frac{1}{c} \partial_t \right) \hat{E}_{\text{sig}}(z,t) \\ = iE_c(z,t) [\beta_{31}\hat{Q}_{31}(z,t)e^{i\frac{\Delta}{2}t} + \beta_{21}\hat{Q}_{21}(z,t)e^{-i\frac{\Delta}{2}t}], \end{aligned} \quad (\text{A15})$$

where $\beta_{i1} = \frac{2\pi N\hbar\kappa_{i1}}{c}$ for $i = \{2, 3\}$.

We now convert the operators to single-excitation wave functions, with $\hat{E}_{\text{sig}}(z,t) \rightarrow E_{\text{sig}}(z,t)$, $\hat{Q}_{21}(z,t) \rightarrow Q_{21}(z,t)$, and $\hat{Q}_{31}(z,t) \rightarrow Q_{31}(z,t)$. Assuming a control field with fixed intensity, applicable for a control field that is long compared to the signal duration, we can analytically solve Eqs. (1)–(3) by applying a Fourier transformation \mathcal{F} to each equation. This results in

$$\begin{aligned} \left(\partial_z + i\frac{\omega}{c} \right) \tilde{E}_{\text{sig}}(z,\omega) &= iE_c\beta_{31}\tilde{Q}_{31}(z,\omega - \Delta/2) \\ &\quad + iE_c\beta_{21}\tilde{Q}_{21}(z,\omega + \Delta/2), \end{aligned} \quad (\text{A16})$$

$$\tilde{Q}_{31}(z,\omega - \Delta/2) = \frac{i\kappa_{13}E_c^*}{i(\omega - \Delta/2) + \Gamma_3} \tilde{E}_{\text{sig}}(z,\omega), \quad (\text{A17})$$

and

$$\tilde{Q}_{21}(z,\omega + \Delta/2) = \frac{i\kappa_{12}E_c^*}{i(\omega + \Delta/2) + \Gamma_2} \tilde{E}_{\text{sig}}(z,\omega), \quad (\text{A18})$$

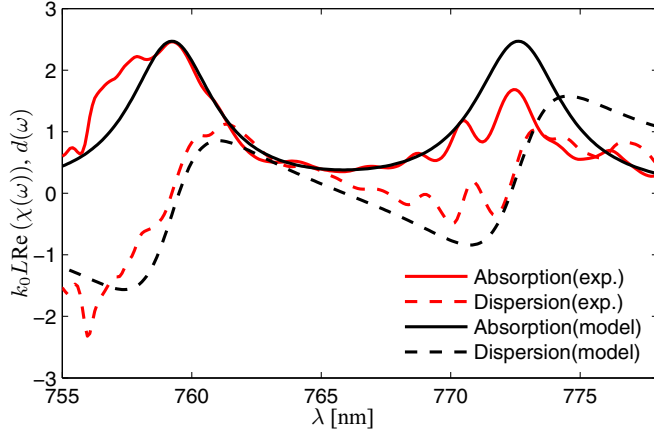


FIG. 5. Plot of measured Raman-induced optical depth of the KTP waveguide (red curve). The measured $\alpha(\omega) = k\text{Im}[\chi(\omega)]$ is used to numerically calculate $\text{Re}[\chi(\omega)]$ via the Kramers-Kronig relation (red dashed curve), where k denotes the wave vector associated to the central wavelength of the signal. The solid (dashed) lines are to show the imaginary (real) part of the response function based on our model; see text for more detail.

where $\tilde{E}_{\text{sig}}(z, \omega) = \mathcal{F}\{E_{\text{sig}}(z, t)\}$, $\tilde{Q}_{31}(z, \omega - \Delta/2) = \mathcal{F}\{Q_{31}(z, t)e^{i\frac{\Delta}{2}t}\}$, and $\tilde{Q}_{21}(z, \omega + \Delta/2) = \mathcal{F}\{Q_{21}(z, t)e^{-i\frac{\Delta}{2}t}\}$. Using Eqs. (A17) and (A18), one can rewrite Eq. (A16) as

$$\left(\partial_z + i\frac{\omega}{c}\right)\tilde{E}_{\text{sig}}(z, \omega) = ik_0\chi(\omega)\tilde{E}_{\text{sig}}(z, \omega), \quad (\text{A19})$$

where

$$\chi(\omega) = \frac{i}{k_0} \left[\frac{c_{13}}{i(\omega - \Delta/2) + \Gamma_3} + \frac{c_{12}}{i(\omega + \Delta/2) + \Gamma_2} \right] \quad (\text{A20})$$

is the linear susceptibility of the Raman transitions, k_0 is the wave vector associated to the central wavelength of the signal, $c_{13} = \kappa_{13}\beta_{31}|E_c|^2$, and $c_{12} = \kappa_{12}\beta_{21}|E_c|^2$. The expected linear dispersion between the two Raman absorption lines can be described by

$$\chi(\omega) \approx \chi(0) + \omega \frac{d\chi}{d\omega} + \dots \quad (\text{A21})$$

Assuming $\Gamma = \Gamma_2 = \Gamma_3$ and $c_1 = c_{12} = c_{13}$, this results in the group delay of

$$\tau_g = \frac{L}{v_g} - \frac{L}{c} = \frac{k_0 L}{2} \frac{d\chi}{d\omega} = \frac{k_0 L}{2} \frac{2c_1(\Delta^2/4 - \Gamma^2)}{(\Gamma^2 + \Delta^2/4)^2}, \quad (\text{A22})$$

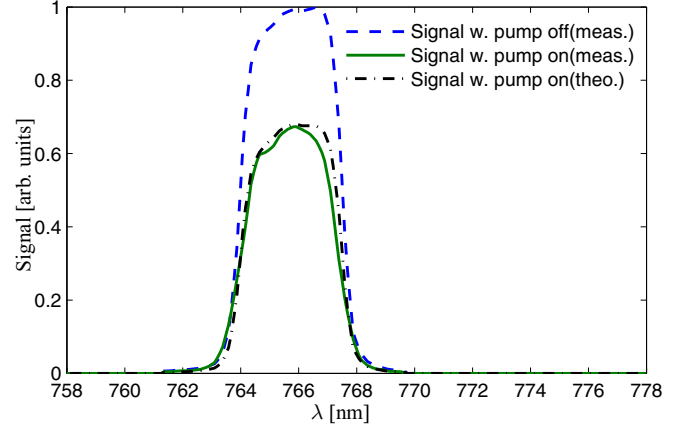


FIG. 6. The output signal spectrum with the control field off (blue dashed curve) and on (green solid curve). The black (dash-dotted) curve is a result of the linear propagation of the signal with the control field off through a medium with a Raman-induced response of $\chi(\omega)$ that has been shown in Fig. 5.

where v_g is the group velocity; the commensurate loss, in dB, is

$$\eta = \frac{10k_0 L}{\ln(10)} \frac{2c_1 \Gamma}{\Gamma^2 + \Delta^2/4}. \quad (\text{A23})$$

Consequently, this leads to a constant delay per dB loss of

$$\frac{\tau}{\eta} = \frac{\ln(10)}{20} \frac{\Delta^2/4 - \Gamma^2}{\Gamma(\Gamma^2 + \Delta^2/4)}. \quad (\text{A24})$$

3. Absorption and dispersion

In addition to our model based on two Raman absorption lines, we can numerically evaluate the real part of the medium's response function. Given that the Raman-induced optical depth can be defined as $d(\omega) = \alpha(\omega)L = -\ln(I_{\text{sig}}^{\text{on}}/I_{\text{sig}}^{\text{off}})$, and $\alpha(\omega)L = k_0 L \text{Im}[\chi(\omega)]$, we can use the Kramers-Kronig relation to evaluate $\text{Re}[\chi(\omega)]$; see Fig. 5.

Using the Raman-induced susceptibility $\chi(\omega)$, which is shown in Fig. 5, we can evaluate the signal field in the frequency domain. The frequency component of the signal field after propagation is given by $\tilde{E}_{\text{sig}}^{\text{on}}(\omega) = \tilde{E}_{\text{sig}}^{\text{off}}(\omega)e^{iL[\omega/c + k_0\chi(\omega)/2]}$, where $\tilde{E}_{\text{sig}}^{\text{off}}(\text{on})$ is the signal spectral field strength with the control pulse off (on). This is shown in Fig. 6, which is in good agreement with the experimental results.

[1] W. Lewins, *Her Majesty's Mails: A History of the Post-Office and an Industrial Account of its Present Condition* (Sampson Low, Son, & Marston, London, 1865).
 [2] H. Kimble, *Nature (London)* **453**, 1023 (2008).
 [3] J. B. Khurgin, *J. Opt. Soc. Am. B* **22**, 1062 (2005).
 [4] J. T. Mok and B. J. Eggleton, *Nature (London)* **433**, 811 (2005).
 [5] Y. Zhao, Y. Zhang, and Q. Wang, *Sens. Actuat. B: Chem.* **173**, 28 (2012).

[6] J. B. Khurgin, *Adv. Opt. Photon.* **2**, 287 (2010).
 [7] H. Schmidt and A. Imamoğlu, *Opt. Lett.* **21**, 1936 (1996).
 [8] M. M. Kash, V. A. Sautenkov, A. S. Zibrov, L. Hollberg, G. R. Welch, M. D. Lukin, Y. Rostovtsev, E. S. Fry, and M. O. Scully, *Phys. Rev. Lett.* **82**, 5229 (1999).
 [9] S. Wang, H. Erlig, H. R. Fetterman, E. Yablonovitch, V. Grubsky, D. S. Starodubov, and J. Feinberg, *IEEE Microwave Guided Wave Lett.* **8**, 327 (1998).
 [10] J. B. Khurgin, *Phys. Rev. A* **62**, 013821 (2000).

- [11] S. Longhi, D. Janner, G. Galzerano, G. Della Valle, D. Gatti, and P. Laporta, *Electron. Lett.* **41**, 1075 (2005).
- [12] C. Madsen and G. Lenz, *IEEE Photon. Technol. Lett.* **10**, 994 (1998).
- [13] M. Notomi, K. Yamada, A. Shinya, J. Takahashi, C. Takahashi, and I. Yokohama, *Phys. Rev. Lett.* **87**, 253902 (2001).
- [14] H. Gersen, T. J. Karle, R. J. P. Engelen, W. Bogaerts, J. P. Korterik, N. F. van Hulst, T. F. Krauss, and L. Kuipers, *Phys. Rev. Lett.* **94**, 073903 (2005).
- [15] Y. A. Vlasov, M. O'Boyle, H. F. Hamann, and S. J. McNab, *Nature (London)* **438**, 65 (2005).
- [16] T. Baba, T. Kawaaski, H. Sasaki, J. Adachi, and D. Mori, *Opt. Express* **16**, 9245 (2008).
- [17] T. Baba, *Nat. Photon.* **2**, 465 (2008).
- [18] R. M. Camacho, M. V. Pack, and J. C. Howell, *Phys. Rev. A* **73**, 063812 (2006).
- [19] R. M. Camacho, M. V. Pack, J. C. Howell, A. Schweinsberg, and R. W. Boyd, *Phys. Rev. Lett.* **98**, 153601 (2007).
- [20] M. R. Vanner, R. J. McLean, P. Hannaford, and A. M. Akulshin, *J. Phys. B* **41**, 051004 (2008).
- [21] N. Akopian, L. Wang, A. Rastelli, O. Schmidt, and V. Zwiller, *Nat. Photon.* **5**, 230 (2011).
- [22] J. S. Wildmann, R. Trotta, J. Martín-Sánchez, E. Zallo, M. O'Steen, O. G. Schmidt, and A. Rastelli, *Phys. Rev. B* **92**, 235306 (2015).
- [23] Y. Okawachi, M. S. Bigelow, J. E. Sharping, Z. Zhu, A. Schweinsberg, D. J. Gauthier, R. W. Boyd, and A. L. Gaeta, *Phys. Rev. Lett.* **94**, 153902 (2005).
- [24] M. González-Herráez, K.-Y. Song, and L. Thévenaz, *Appl. Phys. Lett.* **87**, 081113 (2005).
- [25] J. Sharping, Y. Okawachi, and A. Gaeta, *Opt. Express* **13**, 6092 (2005).
- [26] K.-J. Boller, A. Imamoglu, and S. E. Harris, *Phys. Rev. Lett.* **66**, 2593 (1991).
- [27] L. V. Hau, S. E. Harris, Z. Dutton, and C. H. Behroozi, *Nature (London)* **397**, 594 (1999).
- [28] M. Fleischhauer, A. Imamoglu, and J. P. Marangos, *Rev. Mod. Phys.* **77**, 633 (2005).
- [29] D. G. England, K. A. G. Fisher, Jean-Philippe W. MacLean, P. J. Bustard, R. Lausten, K. J. Resch, and B. J. Sussman, *Phys. Rev. Lett.* **114**, 053602 (2015).
- [30] D. G. England, P. J. Bustard, J. Nunn, R. Lausten, and B. J. Sussman, *Phys. Rev. Lett.* **111**, 243601 (2013).
- [31] T. Sasaki, Y. Yamamoto, and M. Koashi, *Nature (London)* **509**, 475 (2014).
- [32] J.-Y. Guan, Z. Cao, Y. Liu, G.-L. Shen-Tu, J. S. Pelc, M. M. Fejer, C.-Z. Peng, X. Ma, Q. Zhang, and J.-W. Pan, *Phys. Rev. Lett.* **114**, 180502 (2015).
- [33] M. Bradler, P. Baum, and E. Riedle, *Appl. Phys. B* **97**, 561 (2009).
- [34] A. Weiner, *Ultrafast Optics* (Wiley, New York, 2009).
- [35] The waveguide was fabricated by AdvR, Inc.
- [36] D. G. England, P. J. Bustard, D. J. Moffatt, J. Nunn, R. Lausten, and B. J. Sussman, *Appl. Phys. Lett.* **104**, 051117 (2014).
- [37] G. A. Massey, T. M. Loehr, L. J. Willis, and J. C. Johnson, *Appl. Opt.* **19**, 4136 (1980).
- [38] V. Pasiskevicius, A. Fragemann, F. Laurell, R. Butkus, V. Smilgevičius, and A. Piskarskas, *Appl. Phys. Lett.* **82**, 325 (2003).
- [39] M. G. Raymer and J. Mostowski, *Phys. Rev. A* **24**, 1980 (1981).
- [40] M. Spanner and P. Brumer, *Phys. Rev. A* **73**, 023810 (2006).
- [41] P. S. J. Russell, P. Hölzer, W. Chang, A. Abdolvand, and J. Travers, *Nat. Photon.* **8**, 278 (2014).
- [42] H. J. McGuinness, M. G. Raymer, C. J. McKinstrie, and S. Radic, *Phys. Rev. Lett.* **105**, 093604 (2010).
- [43] K. A. G. Fisher, D. G. England, J.-P. W. MacLean, P. J. Bustard, K. J. Resch, and B. J. Sussman, [arXiv:1509.05098](https://arxiv.org/abs/1509.05098).
- [44] M. Hosseini, B. Sparkes, G. Hétet, J. Longdell, P. Lam, and B. Buchler, *Nature (London)* **461**, 241 (2009).
- [45] E. Saglamyurek, N. Sinclair, J. A. Slater, K. Heshami, D. Oblak, and W. Tittel, *New J. Phys.* **16**, 065019 (2014).
- [46] E. Knill, R. Laflamme, and G. J. Milburn, *Nature (London)* **409**, 46 (2001).